Hamiltonian magnetic reconnection with parallel electron heat flux dynamics

D Grasso, E Tassi

Hamiltonian magnetic reconnection with parallel electron heat flux dynamics

D. Grasso[1,2], E. Tassi[3]

[1] Istituto dei Sistemi Complessi - CNR, Via dei Taurini 19, 00185, Roma, Italy
[2] Dipartimento Energia, Politecnico di Torino, Corso Duca degli Abruzzi 24, 10129, Torino, Italy
[3] Aix-Marseille Université, Université de Toulon, CNRS, CPT, UMR 7332, 13288 Marseille, France

(Received 4 May 2015)

We analyze, both analytically and numerically, a two-dimensional six-field fluid model for collisionless magnetic reconnection, accounting for temperature and heat flux fluctuations along the direction of the magnetic guide field. We show that the model possesses a Hamiltonian structure with a noncanonical Poisson bracket. This bracket is characterized by the presence of six infinite families of Casimirs, associated with Lagrangian invariants. This reveals that the model can be reformulated as a system of advection equations, thus generalizing previous results obtained for Hamiltonian isothermal fluid models for reconnection. Numerical simulations indicate that the presence of heat flux and temperature fluctuations yields slightly larger growth rates and similar saturated island amplitudes, with respect to the isothermal models. For values of the sonic Larmor radius much smaller than the electron skin depth, heat flux fluctuations tend to be suppressed and temperature fluctuations follow density fluctuations. Increasing the sonic Larmor radius results in an increasing fraction of magnetic energy converted into heat flux, at the expense of temperature fluctuations. In particular, heat flux fluctuations tend to become relevant along the magnetic island separatrices. The qualitative structures associated with the electron field variables are also reinterpreted in terms of the rotation of the Lagrangian invariants of the system.

1. Introduction

Magnetic reconnection consists of a modification of the topology of a magnetic field in a plasma and is one of the most promising candidates to explain the rapid thermal and kinetic energy releases occurring in phenomena such as solar flares, magnetic substorms and sawtooth oscillations in tokamaks (Priest & Forbes 2000; Biskamp 2000; Yamada *et al.* 2010)). In weakly collisional plasmas, such as those present in the magnetosphere and in tokamak cores, magnetic reconnection can often be triggered by non-dissipative mechanisms. In particular, in such plasmas, finite electron inertia can provide an effective non-dissipative mechanism to break the magnetic frozen-in condition and therefore allow for magnetic reconnection to take place (Coppi 1964).

A considerable effort has been devoted to the modelling of magnetic reconnection mediated by electron inertia (often referred to as "inertial reconnection") by means of fluid models. The literature on the subject is vast and we indicate Refs. (Biskamp 2000) and (Yamada *et al.* 2010) as well as the works cited therein, for the description of applications and limitations of such models. Given its non-dissipative nature, models aiming at describing inertial reconnection are supposed to have Hamiltonian character. This has naturally motivated an effort, originated with Ref. (Schep *et al.* 1994), for deriving

Hamiltonian fluid models for inertial reconnection in slab geometry, in particular in the presence of a strong magnetic guide field. The knowledge of the Hamiltonian structure, in addition to providing an unambiguous expression for the total conserved energy for the system, has offered means to gain further insights on the reconnection dynamics. For instance, the existence of alternative topological constraints on the reconnection process has been unveiled, thanks to the knowledge of the Casimir invariants associated with the Hamiltonian structure (Cafaro *et al.* 1998). The presence of such invariants also helped in understanding the formation of small scale structures in vorticity and current density fields in the nonlinear phase of the reconnection process (Grasso *et al.* 2001). The role of such invariants in inhibiting secondary fluid instabilities has been discussed in Refs. (Del Sarto *et al.* 2006; Grasso *et al.* 2009). Stability conditions and the presence of negative energy modes for equilibria of inertial reconnection fluid models (Kuvshinov *et al.* 1994; Tassi *et al.* 2008) have also been derived, making use of the Energy-Casimir method, which is based on the noncanonical Poisson brackets of the models (see, e.g. Refs. (Morrison 1998; Holm *et al.* 1985)).

To the best of our knowledge, all fluid models, with a known Hamiltonian structure, adopted so far to investigate inertial reconnection, evolve at most two fluid moments for each particle species and assume simple closure relations, of either isothermal or adiabatic type, for the pressure perturbations in the direction along the magnetic guide field. A natural question concerns then the derivation of more refined Hamiltonian fluid models for inertial reconnection that could describe the evolution of higher order moments, such as heat fluxes. In particular, for weakly collisional low-β plasmas (where we indicate with β the ratio between thermal and magnetic pressure, the latter based on the guide field), the limitations of isothermal closures for the electron fluid have been pointed out (de Blank 2001; Zocco & Schekochihin 2011).

The purpose of the present paper is two-fold. First, we present a Hamiltonian six-field fluid model for inertial reconnection, coupling the evolution of an isothermal ion fluid, retaining finite Larmor radius effects, with that of an electron fluid characterized by a non-isothermal closure accounting for parallel temperature and heat flux evolutions. In the second place, we intend to make use of this model, and of its Hamiltonian structure, to investigate some characteristic features of inertial reconnection such as linear growth rates, widths of the macroscopic magnetic island and energy redistribution. We also intend to compare the results obtained from the six-field model with those obtained from a previous Hamiltonian four-field model with isothermal electrons (Waelbroeck & Tassi 2012). This could provide information on the role played by temperature and heat fluxes in inertial reconnection in the framework of a Hamiltonian fluid description. The present investigation aims then at progressing in the description of inertial reconnection in the framework of Hamiltonian fluid models. Clearly, the role of higher order moments in collisionless reconnection has also been investigated with alternative approaches. For instance, investigations by means of a kinetic model have proved the relevance of electron heat flux contributions to the electric field in a region with the size of the order of the electron Larmor radius surrounding the null point (Hesse *et al.* 2004). Also, a hybrid fluid/kinetic model has been adopted to analyze the transfer of energy to higher order moments and the role of dissipation, in inertial reconnection, due to electron Landau damping (Loureiro *et al.* 2013).

The paper is organized as follows. In Sec. 2 the six-field model is introduced and in Sec. 3 its Hamiltonian structure is presented and discussed. Sec. 4 presents a comparison between the six-field model and the isothermal four-field model. In Sec. 5 the role of the sound Larmor radius parameter on the dynamics of temperature and heat flux is

investigated numerically, whereas Sec. 6 describes a qualitative reinterpretation of the field structures in terms of Lagrangian invariants. We conclude in Sec. 7.

2. Model equations

In a Cartesian coordinate system (x, y, z) the model consists of the evolution equations

$$\frac{\partial n_e}{\partial t} + [\phi, n_e] - [A, u_e] = 0, \tag{2.1}$$

$$\frac{\partial F}{\partial t} + [\phi, F] + \rho_s^2[A, T_\parallel + n_e] = 0, \tag{2.2}$$

$$\frac{\partial T_\parallel}{\partial t} + [\phi, T_\parallel] - 2[A, q_\parallel + u_e] = 0, \tag{2.3}$$

$$\frac{\partial q_\parallel}{\partial t} + [\phi, q_\parallel] - \frac{3}{2}\frac{\rho_s^2}{d_e^2}[A, T_\parallel] = 0, \tag{2.4}$$

$$\frac{\partial n_i}{\partial t} + [\Phi, n_i] + [u_i, \mathcal{A}] = 0, \tag{2.5}$$

$$\frac{\partial D}{\partial t} + [\Phi, D] + \rho_i^2[n_i, \mathcal{A}] = 0, \tag{2.6}$$

complemented by the quasi-neutrality relation

$$\frac{\Gamma_0 - 1}{\rho_i^2}\phi + \Gamma_0^{1/2} n_i - n_e = 0 \tag{2.7}$$

and by Ampère's law

$$\nabla^2 A + \Gamma_0^{1/2} u_i - u_e = 0. \tag{2.8}$$

In Eqs. (2.1)-(2.6) $n_{i,e}$ are the guiding center and electron density fluctuations with respect to a constant uniform density background n_0, ϕ is the electrostatic potential and A is the magnetic flux function. The expression of the corresponding magnetic field is given by $\mathbf{B} = \nabla A \times \hat{z} + B\hat{z}$, with B indicating the amplitude of the constant and uniform guide field. The fields F and D are defined as $F = A - d_e^2 u_e$ and $D = \mathcal{A} + d_i^2 u_i$, with $d_{i,e}$ and $u_{i,e}$ indicating the ion and electron skin depths and fluid velocities along the guide field, respectively. The gyroaveraged magnetic flux function and electrostatic potential are defined as $\mathcal{A} = \Gamma_0^{1/2} A$ and $\Phi = \Gamma_0^{1/2}\phi$, where the operator Γ_0 corresponds, in Fourier space, to the multiplication times $I_0(k_\perp^2\rho_i^2)\exp(-k_\perp^2\rho_i^2)$, with I_0 indicating the modified Bessel function of order zero and $k_\perp^2 = k_x^2 + k_y^2$ indicating the squared wave number in the xy plane. The constants $\rho_{i,s}$ represent the thermal ion Larmor radius and the sonic Larmor radius, respectively. The fields $T_\parallel$ and $q_\parallel$, on the other hand, indicate the fluctuations of the electron parallel temperature and heat flux, respectively. Finally, the bracket $[\,,\,]$ is defined as $[f, g] = \partial_x f \partial_y g - \partial_y f \partial_x g$, for two functions f and g.

The above defined quantities are dimensionless and their relation with dimensional quantities is the following:

$$\begin{gathered} t = \frac{v_A}{L}\hat{t}, \qquad x = \frac{\hat{x}}{L}, \qquad d_{i,e} = \frac{\hat{d}_{i,e}}{L}, \qquad \rho_{i,s} = \frac{\hat{\rho}_{i,s}}{L}, \\ n_{i,e} = \frac{L}{\hat{d}_i}\frac{\hat{n}_{i,e}}{n_0}, \qquad u_{i,e} = \frac{L}{\hat{d}_i}\frac{\hat{u}_{i,e}}{v_A}, \qquad A = \frac{\hat{A}_\parallel}{BL}, \qquad \phi = \frac{\hat{\phi}}{BLv_A}, \\ T_\parallel = \frac{L}{\hat{d}_i}\frac{\hat{T}_\parallel}{T_0}, \qquad q_\parallel = \frac{L}{\hat{d}_i}\frac{\hat{q}_\parallel}{n_0 v_A T_0} \end{gathered} \tag{2.9}$$

with L, n_0, T_0 and v_A representing a characteristic scale length, the equilibrium uniform density and electron temperature and the Alfvén speed based on B, respectively. In Eq. (2.9) we indicated with carets the dimensional quantities.

The fields $n_i, n_e, F, D, T_\parallel$ and $q_\parallel$ are supposed to possess translational invariance along the z coordinate, although the extension to a three-dimensional model, under the assumption of a strong guide field, is straightforward.

The six-field model (2.1)-(2.8) represents an extension of the four-field gyrofluid model derived and investigated in Refs. (Waelbroeck & Tassi 2012; Comisso *et al.* 2012). Indeed, the four-field assumed an isothermal closure for the electron fluid, whereas the six-field model allows for an evolution of the parallel electron temperature and heat flux. On the other hand, the six-field model can be seen as a simplified version of the gyrofluid models of Refs. (Scott 2010; Snyder & Hammet 2001) when parallel dynamics, background inhomogeneities, dissipation and moments involving the perpendicular velocities are neglected. Also, our six-field model assumes an isothermal ion fluid and standard closures for the gyroaveraging operators. Electron inertia, which provides the mechanism for magnetic reconnection, is retained, as in Ref. (Scott 2010), but unlike Ref. (Snyder & Hammet 2001). Upon denoting with β_e the β parameter referred to the electron pressure, and with M and m_e the ion and electron mass, respectively, we can recall the relation $\rho_s^2/d_e^2 = (1/2)\beta_e(M/m_e)$. Therefore, as a consequence of retaining finite electron inertia, the ratio between ρ_s and d_e corresponds to determining the β_e parameter.

3. Hamiltonian structure of the model

In this Section we show that the six-field model admits a Hamiltonian formulation. This amounts to show that the evolution equations (2.1)-(2.6), taking into account also Eqs. (2.7) and (2.8), can be cast in the form

$$\frac{\partial \chi_i}{\partial t} = \{\chi_i, H\}, \qquad i = 1, \cdots, 6, \tag{3.1}$$

where the fields $\{\chi_i\}_{i=1,\cdots,6}$ are six appropriate dynamical variables, H is the Hamiltonian functional and $\{\,,\,\}$ is a Poisson bracket.

Given the formulation of the model (2.1)-(2.6), a natural choice for the six dynamical variables corresponds to $\chi_1 = n_e$, $\chi_2 = F$, $\chi_3 = T_\parallel$, $\chi_4 = q_\parallel$, $\chi_5 = n_i$ and $\chi_6 = D$.

With regard to the Hamiltonian, a good candidate is provided by the functional

$$H = \frac{1}{2}\int d^2x \left(\rho_i^2 n_i^2 + \rho_s^2 n_e^2 + d_i^2 u_i^2 + d_e^2 u_e^2 - A\nabla^2 A + \Phi n_i - \phi n_e + \frac{\rho_s^2}{2} T_\parallel^2 + \frac{2}{3} d_e^2 q_\parallel^2\right). \tag{3.2}$$

This quantity has indeed been shown to be conserved by the model equations (Scott 2010), which is a necessary condition for it to be the Hamiltonian of the system. We remark also that the functional (3.2) can be seen as the sum of the Hamiltonian of the four-field model of Ref. (Comisso *et al.* 2012), corresponding to the first seven terms accounting for kinetic, internal and electromagnetic energy, with the internal energy associated with temperature and heat flux fluctuations, provided by the last two terms.

Concerning the Poisson bracket, the structure of the model equations suggests that it be of the form

$$\{\mathcal{F}, \mathcal{G}\} = \sum_{i,j,k=1}^{6} W_k^{ij} \int d^2x \chi_k [\mathcal{F}_{\chi_i}, \mathcal{G}_{\chi_j}], \tag{3.3}$$

where W_k^{ij} are constant coefficients and subscripts on functionals indicate functional

derivatives, so that $\mathcal{F}_{\chi_i} = \delta\mathcal{F}/\delta\chi_i$. We recall that a Poisson bracket is an operation that has to satisfy bilinearity, the Leibniz identity, antisymmetry and the Jacobi identity. The first two of these properties are automatically satisfied by a bracket of the form (3.3). Antisymmetry and the Jacobi identity, on the other hand, impose constraints on the coefficients W_k^{ij}. In particular, as shown in Ref. (Thiffeault & Morrison 2000), for antisymmetry to be satisfied the coefficients must be symmetric in their upper indices, that is

$$W_k^{ij} = W_k^{ji}. \tag{3.4}$$

The Jacobi identity, on the other hand, is satisfied if and only if the matrices $W^{(j)}$ pairwise commute. These matrices are defined as

$$[W^{(j)}]_k^i = W_k^{ij}, \qquad j = 1, \cdots, 6, \tag{3.5}$$

with k labelling rows and i labelling columns. Relying on this result, we can proceed to construct the Poisson bracket following the same procedure adopted in the case of other reduced plasma models (see, e.g. Refs. (Hazeltine *et al.* 1987; Waelbroeck *et al.* 2004; Tassi *et al.* 2008)). More precisely, we can look for a set of six matrices W^j satisfying (3.4)-(3.5) and such that the corresponding equations of motion

$$\frac{\partial \chi_i}{\partial t} = \sum_{j,k=1}^{6} W_k^{ij}[H_{\chi_j}, \chi_k], \qquad i = 1, \cdots, 6, \tag{3.6}$$

obtained using (3.1), (3.2) and (3.3), match the evolution equations (2.1)-(2.6).

With the help of the relations

$$H_{n_e} = \rho_s^2 n_e - \phi, \qquad H_F = -u_e, \qquad H_{T_\parallel} = \frac{\rho_s^2}{2} T_\parallel, \tag{3.7}$$

$$H_{q_\parallel} = \frac{2}{3} d_e^2 q_\parallel, \qquad H_{n_i} = \rho_i^2 n_i + \Phi, \qquad H_D = u_i, \tag{3.8}$$

one finds that the set of pairwise commuting matrices $W^{(j)}$ yielding a Poisson bracket as well as the desired equations of motion can be written as

$$W^{(1)} = \begin{pmatrix} 1 & 0 & 0 & 0 & 0 & 0 \\ 0 & 1 & 0 & 0 & 0 & 0 \\ 0 & 0 & 1 & 0 & 0 & 0 \\ 0 & 0 & 0 & 1 & 0 & 0 \\ 0 & 0 & 0 & 0 & 0 & 0 \\ 0 & 0 & 0 & 0 & 0 & 0 \end{pmatrix}, \qquad W^{(2)} = \begin{pmatrix} 0 & \rho_s^2 d_e^2 & 0 & 0 & 0 & 0 \\ 1 & 0 & 2 & 0 & 0 & 0 \\ 0 & \rho_s^2 d_e^2 & 0 & -3\rho_s^2/2 & 0 & 0 \\ 0 & 0 & -2d_e^2 & 0 & 0 & 0 \\ 0 & 0 & 0 & 0 & 0 & 0 \\ 0 & 0 & 0 & 0 & 0 & 0 \end{pmatrix},$$

$$W^{(3)} = \begin{pmatrix} 0 & 0 & 2 & 0 & 0 & 0 \\ 0 & 2 & 0 & -3/d_e^2 & 0 & 0 \\ 1 & 0 & 4 & 0 & 0 & 0 \\ 0 & -2d_e^2 & 0 & 2 & 0 & 0 \\ 0 & 0 & 0 & 0 & 0 & 0 \\ 0 & 0 & 0 & 0 & 0 & 0 \end{pmatrix}, \qquad W^{(4)} = \begin{pmatrix} 0 & 0 & 0 & 3\rho_s^2/(2d_e^2) & 0 & 0 \\ 0 & 0 & -3/d_e^2 & 0 & 0 & 0 \\ 0 & -3\rho_s^2/2 & 0 & 3\rho_s^2/(2d_e^2) & 0 & 0 \\ 1 & 0 & 2 & 0 & 0 & 0 \\ 0 & 0 & 0 & 0 & 0 & 0 \\ 0 & 0 & 0 & 0 & 0 & 0 \end{pmatrix},$$

$$W^{(5)} = \begin{pmatrix} 0 & 0 & 0 & 0 & 0 & 0 \\ 0 & 0 & 0 & 0 & 0 & 0 \\ 0 & 0 & 0 & 0 & 0 & 0 \\ 0 & 0 & 0 & 0 & 0 & 0 \\ 0 & 0 & 0 & 0 & -1 & 0 \\ 0 & 0 & 0 & 0 & 0 & -1 \end{pmatrix}, \qquad W^{(6)} = \begin{pmatrix} 0 & 0 & 0 & 0 & 0 & 0 \\ 0 & 0 & 0 & 0 & 0 & 0 \\ 0 & 0 & 0 & 0 & 0 & 0 \\ 0 & 0 & 0 & 0 & 0 & 0 \\ 0 & 0 & 0 & 0 & 0 & -\rho_i^2 d_i^2 \\ 0 & 0 & 0 & 0 & -1 & 0 \end{pmatrix} \tag{3.9}$$

From Eqs. (3.3) and (3.9) it follows then that the Poisson bracket for the model (2.1)-(2.6) is given by

$$\{\mathcal{F},\mathcal{G}\} = \{\mathcal{F},\mathcal{G}\}_e + \{\mathcal{F},\mathcal{G}\}_i, \tag{3.10}$$

where

$$\begin{aligned}
\{\mathcal{F},\mathcal{G}\}_e = \int d^2x \Bigg[& n_e \left([\mathcal{F}_{n_e},\mathcal{G}_{n_e}] + \rho_s^2 d_e^2 [\mathcal{F}_F,\mathcal{G}_F] + 2[\mathcal{F}_{T_\parallel},\mathcal{G}_{T_\parallel}] + \frac{3}{2}\frac{\rho_s^2}{d_e^2}[\mathcal{F}_{q_\parallel},\mathcal{G}_{q_\parallel}] \right) \\
& + F \left([\mathcal{F}_F,\mathcal{G}_{n_e}] + [\mathcal{F}_{n_e},\mathcal{G}_F] + 2([\mathcal{F}_F,\mathcal{G}_{T_\parallel}] + [\mathcal{F}_{T_\parallel},\mathcal{G}_F]) - \frac{3}{d_e^2}([\mathcal{F}_{q_\parallel},\mathcal{G}_{T_\parallel}] + [\mathcal{F}_{T_\parallel},\mathcal{G}_{q_\parallel}]) \right) \\
& + T_\parallel \left([\mathcal{F}_{T_\parallel},\mathcal{G}_{n_e}] + [\mathcal{F}_{n_e},\mathcal{G}_{T_\parallel}] + \rho_s^2 d_e^2 [\mathcal{F}_F,\mathcal{G}_F] \right. \\
& \left. - \frac{3}{2}\rho_s^2([\mathcal{F}_{q_\parallel},\mathcal{G}_F] + [\mathcal{F}_F,\mathcal{G}_{q_\parallel}]) + 4[\mathcal{F}_{T_\parallel},\mathcal{G}_{T_\parallel}] + \frac{3}{2}\frac{\rho_s^2}{d_e^2}[\mathcal{F}_{q_\parallel},\mathcal{G}_{q_\parallel}] \right) \\
& + q_\parallel \left([\mathcal{F}_{q_\parallel},\mathcal{G}_{n_e}] + [\mathcal{F}_{n_e},\mathcal{G}_{q_\parallel}] - 2d_e^2([\mathcal{F}_{T_\parallel},\mathcal{G}_F] + [\mathcal{F}_F,\mathcal{G}_{T_\parallel}]) + 2([\mathcal{F}_{q_\parallel},\mathcal{G}_{T_\parallel}] + [\mathcal{F}_{T_\parallel},\mathcal{G}_{q_\parallel}]) \right) \Bigg]
\end{aligned} \tag{3.11}$$

$$\{\mathcal{F},\mathcal{G}\}_i = -\int d^2x \left(n_i \left([\mathcal{F}_{n_i},\mathcal{G}_{n_i}] + \rho_i^2 d_i^2 [\mathcal{F}_D,\mathcal{G}_D] \right) + D\left([\mathcal{F}_D,\mathcal{G}_{n_i}] + [\mathcal{F}_{n_i},\mathcal{G}_D] \right) \right). \tag{3.12}$$

As in the case of its isothermal reduction of Ref. (Waelbroeck & Tassi 2012), also this model possesses a Poisson bracket with a direct sum structure, given that the brackets $\{\,,\,\}_e$ and $\{\,,\,\}_i$ are Poisson brackets of their own and that the corresponding Hamiltonian operators are functions of independent sets of variables. These two brackets evolve independently the electron and ion fluid variables, the coupling between which being provided by the Hamiltonian (3.2). In particular, the bracket $\{\,,\,\}_i$ is already present in the direct sum for the Poisson bracket of the isothermal model (Waelbroeck & Tassi 2012).

Solutions $\mathcal{C}$ of the equation

$$\{\mathcal{C},\mathcal{F}\} = 0, \tag{3.13}$$

valid for any functional $\mathcal{F}$ of the dynamical variables, are Casimir invariants of the system. These functionals foliate the phase space and are preserved by the dynamics (see, e.g. Ref. (Morrison 1998)). For the Poisson bracket (3.10) they correspond to the following six infinite families of functionals:

$$C_i = \int d^2x \mathcal{C}_i(G_i), \qquad i = 1,\cdots,4, \tag{3.14}$$

$$C_\pm = \int d^2x \mathcal{C}_\pm(I_\pm), \tag{3.15}$$

where

$$G_1 = F - \frac{d_e\rho_s}{\sqrt{3+\sqrt{6}}} n_e - d_e\rho_s \sqrt{\frac{1}{2}+\frac{1}{\sqrt{6}}} T_\parallel - d_e^2\sqrt{\frac{2}{3}} q_\parallel, \tag{3.16}$$

$$G_2 = F + \frac{d_e\rho_s}{\sqrt{3+\sqrt{6}}} n_e + d_e\rho_s \sqrt{\frac{1}{2}+\frac{1}{\sqrt{6}}} T_\parallel - d_e^2\sqrt{\frac{2}{3}} q_\parallel, \tag{3.17}$$

$$G_3 = F + \frac{d_e\rho_s}{\sqrt{3-\sqrt{6}}} n_e - d_e\rho_s \sqrt{\frac{1}{2}-\frac{1}{\sqrt{6}}} T_\parallel + d_e^2\sqrt{\frac{2}{3}} q_\parallel, \tag{3.18}$$

$$G_4 = F - \frac{d_e\rho_s}{\sqrt{3-\sqrt{6}}} n_e + d_e\rho_s \sqrt{\frac{1}{2}-\frac{1}{\sqrt{6}}} T_\parallel + d_e^2\sqrt{\frac{2}{3}} q_\parallel, \tag{3.19}$$

$$I_\pm = D \pm d_i\rho_i n_i, \tag{3.20}$$

and where $\mathcal{C}_{1,2,3,4}$ and $\mathcal{C}_{\pm}$ are arbitrary functions. The Casimirs $C_{1,2,3,4}$ and the Casimirs $C_{\pm}$ derive from the brackets $\{\ ,\ \}_e$ and $\{\ ,\ \}_i$, respectively.

The infinite families of Casimirs are associated with Lagrangian invariants of the model. Indeed, if one performs the change of variables $(n_e, F, T_{\parallel}, q_{\parallel}, n_i, D) \to (G_1, G_2, G_3, G_4, I_+, I_-)$ the model equations (2.1)-(2.6) take the remarkable form

$$\begin{aligned} \frac{\partial G_i}{\partial t} &= -[\phi_i, G_i], \qquad i = 1, \cdots, 4, \\ \frac{\partial I_{\pm}}{\partial t} &= -[\Phi_{\pm}, I_{\pm}], \end{aligned} \tag{3.21}$$

where

$$\begin{aligned} &\phi_1 = \phi - \sqrt{3+\sqrt{6}}\frac{\rho_s}{d_e}A, \qquad \phi_2 = \phi + \sqrt{3+\sqrt{6}}\frac{\rho_s}{d_e}A, \\ &\phi_3 = \phi + \sqrt{3-\sqrt{6}}\frac{\rho_s}{d_e}A, \qquad \phi_4 = \phi - \sqrt{3-\sqrt{6}}\frac{\rho_s}{d_e}A, \\ &\Phi_{\pm} = \Phi \mp \frac{\rho_i}{d_i}\mathcal{A}, \end{aligned} \tag{3.22}$$

The six Lagrangian invariants $G_1, G_2, G_3, G_4, I_+, I_-$ represent "normal" variables (Tassi *et al.* 2010) for the bracket (3.10).

From Eqs. (3.21) one then sees that the dynamics of the reconnection model (2.1)-(2.6) actually expresses the advection of six Lagrangian invariants transported by incompressible flows associated with the stream functions (3.22). Such stream functions are reminiscent of those advecting the generalized perturbed distribution functions in the 2D gyrokinetic description from which the model can be derived from (Scott 2010). Such stream functions are linear combinations of the electrostatic and magnetic potential, or of their gyroaveraged versions in the case of $\Phi_{\pm}$. This has its origin at the guiding center level, where such potentials are associated with the $\mathbf{E}\times\mathbf{B}$ drift and with the free stream of the guiding centers along the poloidal magnetic field.

Lagrangian invariant dynamics underlying collisionless reconnection is a feature observed in earlier Hamiltonian models for reconnection, where isothermal closures were adopted (Cafaro *et al.* 1998; Grasso *et al.* 2000; Waelbroeck *et al.* 2009; Waelbroeck & Tassi 2012). For such models, the connections with drift or gyro-kinetic dynamics had been pointed out in Refs.(de Blank 2001; Liseikina *et al.* 2004; Pegoraro *et al.* 2005a,b; Comisso *et al.* 2012; Tassi 2014a,b). The above Hamiltonian structure and the formulation (3.21) of the model, show that, when going beyond the isothermal closure and imposing for the electrons a fluid closure consistent with that adopted in Refs. (Scott 2010; Snyder & Hammet 2001) in the non-dissipative limit, the model still preserves a Hamiltonian structure and its dynamics still can be entirely interpreted in terms of Lagrangian invariants. We recall that the model (2.1)-(2.6) can be derived from the following gyrokinetic system, written in dimensional form:

$$\frac{\partial g_i}{\partial t} + \frac{c}{B}\left[J_0\left(\phi - \frac{v}{c}A\right), g_i\right] = 0, \tag{3.23}$$

$$\frac{\partial g_e}{\partial t} + \frac{c}{B}\left[\phi - \frac{v}{c}A, g_e\right] = 0. \tag{3.24}$$

Eqs. (3.23)-(3.24) are coupled with the quasi-neutrality relation

$$\frac{e^2 n_0}{T_i}(\Gamma_0 - 1)\phi + e\int d\mathcal{W}(J_0 g_i - g_e) = 0, \tag{3.25}$$

and Ampère's law

$$\nabla^2 A - 4\pi \frac{e^2}{c^2} n_0 \left(\frac{\Gamma_0}{m_i} + \frac{1}{m_e} \right) A + 4\pi \frac{e}{c} \int d\mathcal{W} v (J_0 g_i - g_e) = 0. \tag{3.26}$$

Eqs. (3.23) and (3.24) govern the evolution of $g_i = f_i + \mathcal{F}_i (e/T_i)(v/c) J_0 A$ and $g_e = f_e - \mathcal{F}_e (e/T_0)(v/c) A$, where e is the proton charge, T_i the ion equilibrium temperature, J_0 the gyroaveraging operator, $f_{i,e}(x, y, z, v, \mu, t)$ indicate the perturbations of the ion and electron equilibrium distribution functions $\mathcal{F}_{i,e}$, respectively, which are defined as

$$\mathcal{F}_i(v, \mu) = n_0 \left(\frac{m_i}{2\pi T_i} \right)^{3/2} \mathrm{e}^{-\frac{m_i v^2 + 2\mu B}{2T_i}}, \qquad \mathcal{F}_e(v, \mu) = n_0 \left(\frac{m_e}{2\pi T_0} \right)^{3/2} \mathrm{e}^{-\frac{m_e v^2 + 2(m_e/m_i)\mu B}{2T_0}}. \tag{3.27}$$

We indicate with v the velocity coordinate along the magnetic guide field direction and with μ the ion magnetic moment. The volume element $d\mathcal{W}$ is defined as $d\mathcal{W} = 2\pi B d\mu dv / m_i$.

The model equations (2.1)-(2.6) can be derived from Eqs. (3.23)-(3.24) by taking moments with respect to the Hermite polynomials in the parallel velocity coordinate, and truncating the resulting fluid system by imposing that the moment of order four, for the electron fluid, and of order two for the ion fluid, be zero (Scott (2010)). The quasi-neutrality relation (3.25) and Ampère's law (3.26) can, on the other hand, be easily identified with Eqs. (2.7) and (2.8), respectively, upon introducing fluid velocities and densities and applying standard gyroaveraging closure rules (Scott (2010)).

The parent gyrokinetic system (3.23)-(3.24) also possesses a Hamiltonian structure (Tassi (2014a)), given by the Hamiltonian functional

$$\begin{aligned} H(g_i, g_e) = \frac{1}{2} \int d^2x d\mathcal{W} \Bigg[& \frac{T_i}{\mathcal{F}_i} g_i^2 + \frac{T_0}{\mathcal{F}_e} g_e^2 + e\phi (J_0 g_i - g_e) \\ & - e \frac{v}{c} A (J_0 g_i - g_e) \Bigg]. \end{aligned} \tag{3.28}$$

and the Poisson bracket

$$\{F, G\} = \frac{c}{eB} \int d^2x d\mathcal{W} \, (-g_i [F_{g_i}, G_{g_i}] + g_e [F_{g_e}, G_{g_e}]). \tag{3.29}$$

The closure adopted to derive the six-field model preserves then the Hamiltonian character of the parent gyrokinetic model. The Hamiltonian (3.2), in particular, can be derived from the gyrokinetic Hamiltonian (3.28) by replacing g_i and g_e with the corresponding truncated expansions in terms of Hermite polynomials. The Casimirs of the gyrokinetic bracket (3.29), on the other hand, are given by

$$C_i = \int d^2x d\mathcal{W} \, \mathcal{C}_i(g_i), \qquad C_e = \int d^2x d\mathcal{W} \, \mathcal{C}_e(g_e), \tag{3.30}$$

with $\mathcal{C}_{i,e}$ arbitrary functions. Upon applying the fluid closure, such two families of gyrokinetic Casimirs transform into the six families of gyrofluid Casimirs (3.14)-(3.15).

We remark that the model (2.1)-(2.6) can easily be upgraded, following for instance Scott (2010), to an eight-field model accounting also for parallel ion temperature and heat flux fluctuations. The two additional equations would be analogous to Eqs. (2.3)-(2.4), but with electron quantities replaced by the corresponding ion quantities, and electrostatic and magnetic potential replaced by their gyroaveraged counterparts. The resulting model would still be Hamiltonian. In the total conserved energy ion and electron quantities would then enter in the same way. The corresponding Poisson bracket would be the direct sum $\{\mathcal{F}, \mathcal{G}\} = \{\mathcal{F}, \mathcal{G}\}_e + \{\mathcal{F}, \mathcal{G}\}_I$, where $\{\mathcal{F}, \mathcal{G}\}_I$ is analogous to $\{\mathcal{F}, \mathcal{G}\}_e$,

but with electron quantities replaced by the corresponding ion quantities. Consequently, the eight-field model would possess eight infinite families of Casimirs associated with Lagrangian invariants. Four families of Casimirs analogous to $C_1, \cdots, C_4$, but for the ion species, would indeed be present. Although the extension to the eight-field model appears to be relatively straightforward, for the present numerical investigation we decided to reserve the refined closure for the electron fluid only. Indeed, for the equilibrium state that we consider, which does not include ion density, velocity or temperature gradients, ion fluctuations appear to have little influence on the inertial reconnection dynamics (see, for instance Grasso *et al.* (2010) and Comisso *et al.* (2012)). Actually, most of the magnetic energy turns out to be converted into electron fluctuations, as will be confirmed also in Sec. 4. Consequently, we stick to the six-field model and postpone the inclusion of ion temperature and heat flux effects to future work, where different equilibrium gradients will be considered.

Incidentally, we remark also that the eight-field model could be reduced to another six-field model by neglecting heat fluxes and thus leaving three pairs of equations for densities, parallel canonical momenta and temperatures of ions and electrons, respectively. Such model would also be Hamiltonian. The Hamiltonian functional would be simply obtained from that of the eight-field model by suppressing heat flux terms. The Poisson bracket would, again be a direct sum of two Poisson brackets, one related to the electron and one to the ion quantities. Such brackets could be obtained from $\{\mathcal{F},\mathcal{G}\}_e$ and $\{\mathcal{F},\mathcal{G}\}_I$ by suppressing all the terms depending on heat fluxes and on functional derivatives with respect to them, and by replacing the factor 4 by a factor 1 in the coefficient multiplying $T_\parallel[\mathcal{F}_{T_\parallel},\mathcal{G}_{T_\parallel}]$ in $\{\mathcal{F},\mathcal{G}\}_e$ (and proceeding analogously with $\{\mathcal{F},\mathcal{G}\}_I$).

4. Comparison with the isothermal closure

As pointed out in section 2 the six-field model equations reduce to the four-field ones when an isothermal behavior for the electrons is considered. In this section we intend to highlight the difference between these two sets of equations, by comparing results from simulations obtained for the same set of parameters. We use here an extended version of the pseudo-spectral numerical code adopted in Ref. (Comisso *et al.* 2012), where the fields of the model are decomposed in a time independent equilibrium and an evolving perturbation which is advanced in time according to a third order Adams-Bashforth algorithm. In order to investigate the evolution of spontaneous magnetic reconnection instabilities, the system of Eqs. (2.1)-(2.6) is solved numerically considering an equilibrium which is linearly unstable with respect to tearing modes. In particular, we adopt the following equilibrium:

$$n_{ieq}(x) = n_{eeq}(x) = n_0, \qquad u_{ieq}(x) = 0, \qquad A_{eq}(x) = \sum_{n=-11}^{11} \hat{f}_n e^{inx}, \tag{4.1}$$

$$T_{\parallel_{eq}} = 0, \qquad q_{\parallel_{eq}} = 0, \tag{4.2}$$

where we recall that n_0 represents a uniform background density, whereas $\hat{f}_n$ are the Fourier coefficients of the function

$$f(x) = A_0/\cosh^2(x) \tag{4.3}$$

with A_0 representing a parameter that determines the strength of the in-plane equilibrium magnetic field. In the following we consider $A_0 = 0.1$ and restrict ourselves to the strongly unstable regime, which is characterized by large values of the standard

instability parameter, Δ' (Furth *et al.* 1963), and which is relevant to the general problem of fast magnetic reconnection. Our integrations domain is fixed by $L_x = 2\pi$ and $L_y = 4\pi$, while for the physical parameters we choose the following values: $d_e = 0.2$, $d_i = 2$, $\rho_i = 0.2$ and $\rho_s = 0.01, 0.1, 0.4$ and 0.8. The first characteristic quantity of the reconnection process that we investigate is the linear growth rate of the perturbation. Figure 1 shows, for different values of ρ_s, a comparison of the growth rate, obtained from numerical simulations of the six-field model and of four-field model. The growth rate is measured as the variation of the perturbed magnetic flux at the X-point. In the same figure the numerical values are also compared against the analytical predictions obtained by applying the asymptotic formula for the linear growth rate γ_L given by $\gamma_L = 0.2 k_y (2 d_e \rho_\tau^2/\pi)^{1/3}$(Porcelli 1991; Fitzpatrick & Porcelli 2004), where $k_y = 2m\pi/L_y$, m is the mode number and $\rho_\tau = \sqrt{\rho_s^2 + \rho_i^2}$. This formula is valid for $\rho_s^2 << d_e^2 (m_i/m_e)^{3/4}$ and for $\Delta' >> \min[1, (d_e/\rho_\tau)^{1/3}]$. We note that the presence of heat flux fluctuations leads to slightly greater growth rates. The increase in the growth rates is in the range of $5 - 7\%$. On the other hand the analytic formula overestimates the growth rates, when compared to both the six- and four field models. The difference is greater for larger values of ρ_s, as it should be expected when increasing the ratio ρ_s/d_e at fixed mass ratio. The similarity in the linear growth rates between the six and four-field model, reflects also in similar magnetic island amplitudes at saturation, in agreement with what is observed when a drift-kinetic description is adopted for the electrons (Loureiro *et al.* 2013). We note that this result refers to the large Δ' regime we are addressing here, and does not extend to small Δ' regimes, when the island saturation amplitude becomes comparable with the kinetics scales, as already pointed out in Ref. (Loureiro *et al.* 2013).
Subsequently we analyze the energy distribution in the two models. Clearly the evolution of the heat flux in the six-field model allows the electron temperature to deviate from the isothermal behavior and opens new energy channels. The different contributions to the total energy are denoted as

$$E_{mag} = \frac{1}{2}\int d^2x\, |\nabla A|^2, \qquad E_{ke} = \frac{d_e^2}{2}\int d^2x\, u_e^2, \qquad E_{ele} = -\frac{1}{2}\int d^2x\, \phi n_e,$$
$$E_{the} = \frac{\rho_s^2}{2}\int d^2x\, n_e^2, \qquad E_{T_\parallel} = \frac{\rho_s^2}{4}\int d^2x\, T_\parallel^2, \qquad E_{q_\parallel} = \frac{d_e^2}{3}\int d^2x\, q_\parallel^2,$$
$$E_{ki} = \frac{d_i^2}{2}\int d^2x\, u_i^2, \qquad E_{eli} = -\frac{1}{2}\int d^2x\, \Phi n_i, \qquad E_{thi} = \frac{\rho_i^2}{2}\int d^2x\, n_i^2.$$

In Fig. 2 a comparison between the relative variations of the different contributions to the total energy is presented for the case where the ion sound Larmor radius is equal to 0.1. The relative variations for each form of energy are calculated with respect to the initial values and normalized with respect to the total energy, so that, for instance, in the case of the magnetic energy one has $\delta E_{mag}(t) = (E_{mag}(t) - E_{mag}(0))/H(0)$, where H is the Hamiltonian functional (3.2). We compare two simulations that were initialized with the same equilibrium configuration and perturbation, hence, the same total energy. The simulations have been stopped when the magnetic island has reached approximately the same macroscopic size. This explains why we find that the behavior of the converted magnetic energy is similar, as shown in the second panel of Fig. 2 (we number the panels starting from the left panel in the top row and attributing odd numbers to panels on the left column and even numbers to those on the right column). In both models the magnetic energy, E_{mag} is mainly converted into electron and ion internal energy, shown in the fifth ans sixth panels. We remark that the main differences occur in the energies involving the electron quantities, *i.e.* E_{ke}, E_{ele} and E_{the} shown in the third, fifth and

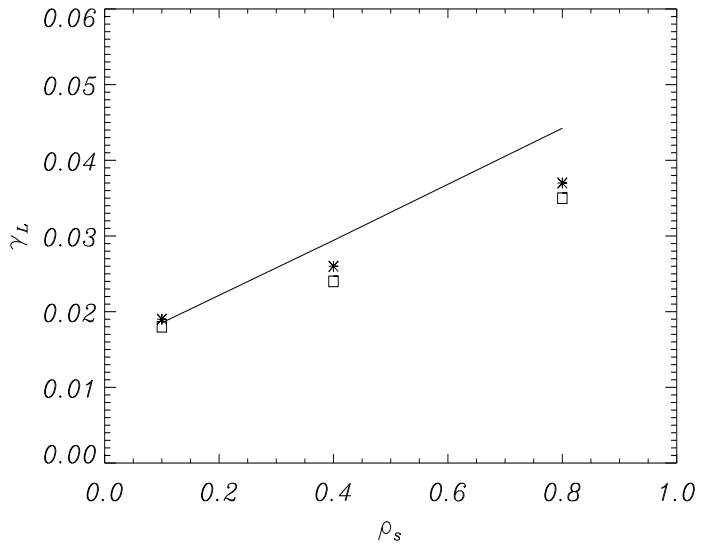

FIGURE 1. Growth rates obtained from the numerical simulations and analytical prediction for different values of ρ_s. Asterisks and squares correspond to results of the six- and four-field simulations, respectively, whereas the solid line refers to the analytical prediction.

seventh panels respectively. The smaller amount of magnetic energy converted into these forms in the six-field model is compensated by the energy conversion into internal energy due to the temperature and heat flux fluctuations, that is $E_{T_\parallel}$, and $E_{q_\parallel}$, shown in the ninth and tenth panels respectively.

5. Dependence on ρ_s

In this section we examine the dependence of some aspects of the dynamics of the six-field model on the sound Larmor radius ρ_s. The motivation for the choice of this parameter is that ρ_s is an appropriate variable to investigate the role of heat flux fluctuations, which is the main new ingredient of the six-field model. Indeed, by varying ρ_s we can study the transition from a regime with negligible heat flux ($\rho_s << d_e$), as is the case with an adiabatic equation of state, to a regime with finite heat flux fluctuations. It is worth to remember that $\rho_s^2/d_e^2 = (1/2)\beta_e(M/m_e)$. In our simulations we kept fixed both the value of $d_e = 0.2$ and the ratio $d_i/d_e = 10$. Hence, the value of ρ_s can also be seen as a measure of the value of the β_e parameter.
Examining the model equations (2.1-2.6) we see that in the limit $\rho_s \ll d_e$ the heat flux equation (2.4) tends to decouple from the system. Because we set the initial heat flux equal to zero, we expect it then not to increase significantly. It hence follows, by comparing Eqs. (2.1) and (2.3), that $n_e \approx T_\parallel/2$, given that $n_e(x, y, 0) = T_\parallel(x, y, 0)/2 = 0$. On the contrary, when increasing the value of ρ_s we expect the heat flux evolution to be not trivial. As a consequence, density and temperature fluctuations are no longer proportional. We illustrate this behavior with the support of the numerical simulations. An example is given in Figs. 3 and 4, where in the left panels we plot the profiles at $y = \pi$, for two different simulation times, of the electron density fluctuations and of half the parallel temperature fluctuations for two cases with $\rho_s = 0.01$ and $\rho_s = 0.4$, respectively. The simulation times are chosen for both cases in the nonlinear phase and close to

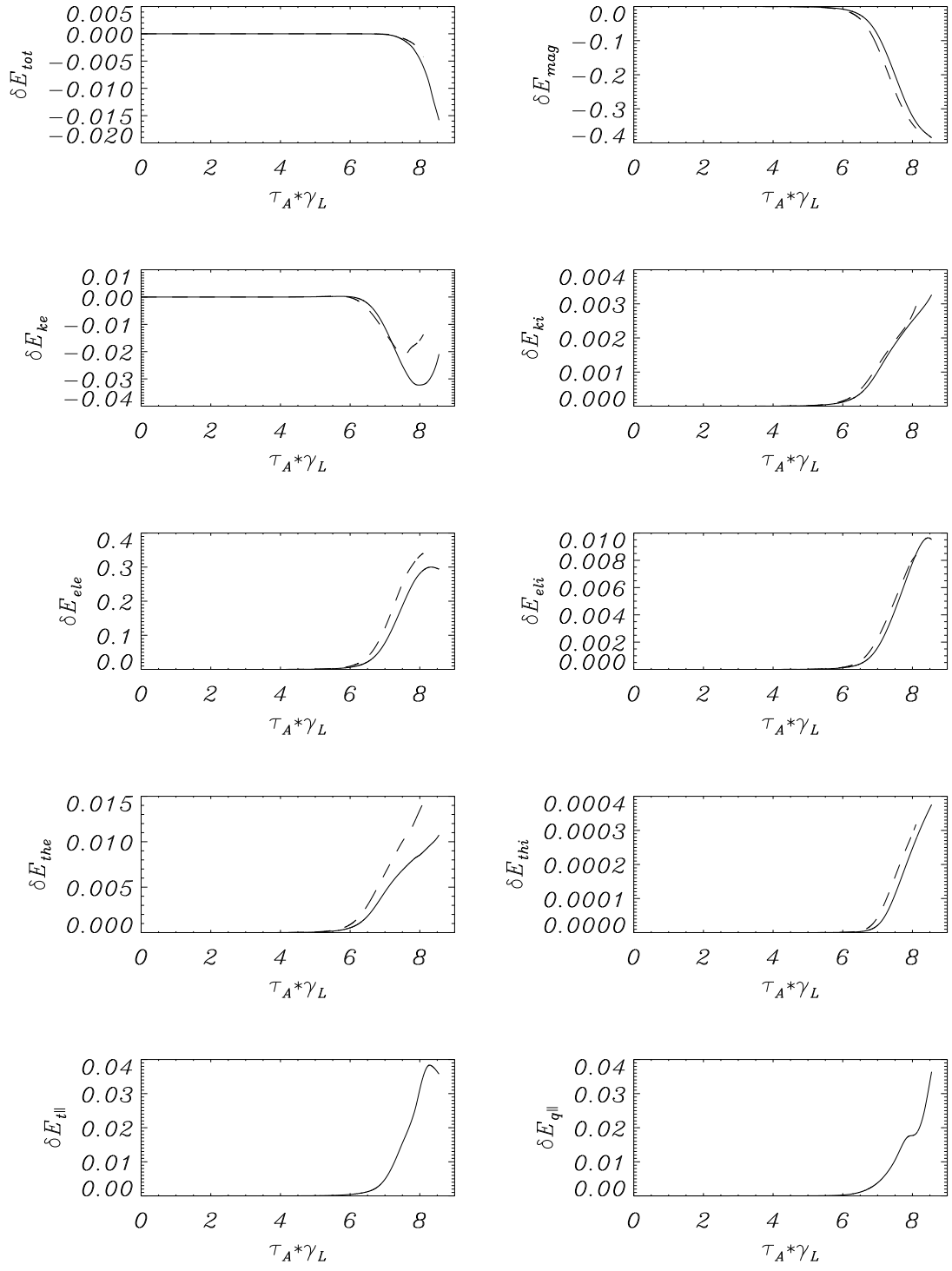

FIGURE 2. Comparison of relative energy variations between the six-field model (solid line) and the four-field model (dashed line) at $\rho_s = 0.1$.

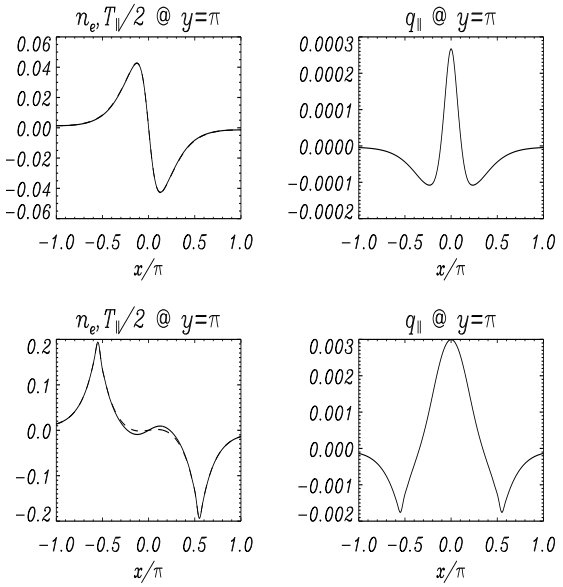

FIGURE 3. Figures on the left-hand side show profiles at $y = \pi$ of fluctuations of the electron density n_e (dashed line) superimposed to those of half the electron temperature $T_\parallel/2$ (solid line). The figures on the right-hand side show the profiles at $y = \pi$ of the heat flux fluctuations $q_\parallel$. All figures refer to the case $\rho_s = 0.01$. The first row corresponds to $t = 325\tau_A$, a simulation time in the nonlinear phase, and the second row corresponds to $t = 400\tau_A$, close to saturation. We indicate with $\tau_A = L/v_A$ the characteristic Alfvén time. In this regime the heat flux fluctuations remain negligible and temperature fluctuations are almost proportional to density fluctuations.

saturation. We see that for small values of ρ_s (Fig. 3) the two curves of n_e and $T_\parallel/2$ are indistinguishable in the nonlinear phase and almost overlap at saturation as well. On the contrary for $\rho_s = 0.4$ (Fig. 4) the density fluctuations are much larger than those of $T_\parallel/2$. In particular, the greatest differences occur in regions where the heat flux fluctuations, shown in the right panel of the same figure, become more pronounced. We observe in particular two positive peaks in $q_\parallel$, which move further apart in time. It turns out that these peaks are located in correspondence with the magnetic island separatrices. Their drift in opposite directions indicates that the peaks are following the separatrices of the growing magnetic island. Further simulations suggest this behavior to be quite generic for sufficiently large ρ_s. Therefore, we can expect heat flux effects, when relevant, to be concentrated along the island separatrices rather than inside the island.

When we examine the role of high values of the ion sound Larmor radius we observe a tendency toward the suppression of temperature fluctuations. This behavior is illustrated through the evolution of the integral quantity $2E_{T_\parallel}/\rho_s^2 = \int d^2x T_\parallel^2/2$ in Fig. 5. We see that between the small and the large ρ_s limits there are approximately three orders of magnitude of difference in the temperature fluctuations. As expected, then, heat flux contributes to distribute the temperature uniformly in space, which reflects into a reduction of temperature fluctuations.

The spatial distribution of temperature fluctuations in the smallest and largest ρ_s cases can be observed from the contour plots shown in Fig. 6. In the small ρ_s limit small scale structures are aligned with the magnetic island separatrix. An identical distribution is observed in the contour plots of n_e (Fig. 8 left panel) and agrees with previous studies of the two-field model of Ref. (Cafaro *et al.* 1998), where density fluctuations were proportional

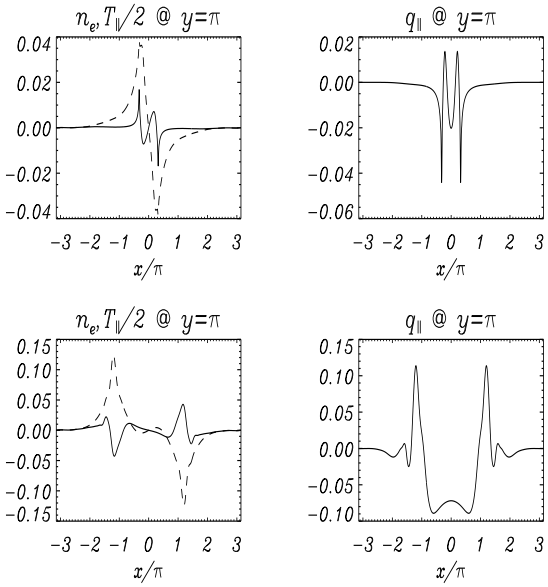

FIGURE 4. The meaning of the figures is the same as in Fig. 3, but here the case $\rho_s = 0.4$ is shown. The first row corresponds to $t = 250\tau_A$, a simulation time in the nonlinear phase, and the second row corresponds to $t = 325\tau_A$, close to saturation. By comparing with Fig. 3 we observe that increasing ρ_s leads to an increase in the heat flux. The highest peaks in the heat flux turn out to be located in correspondence with the island separatrices. As a consequence, temperature fluctuations no longer follow density fluctuations.

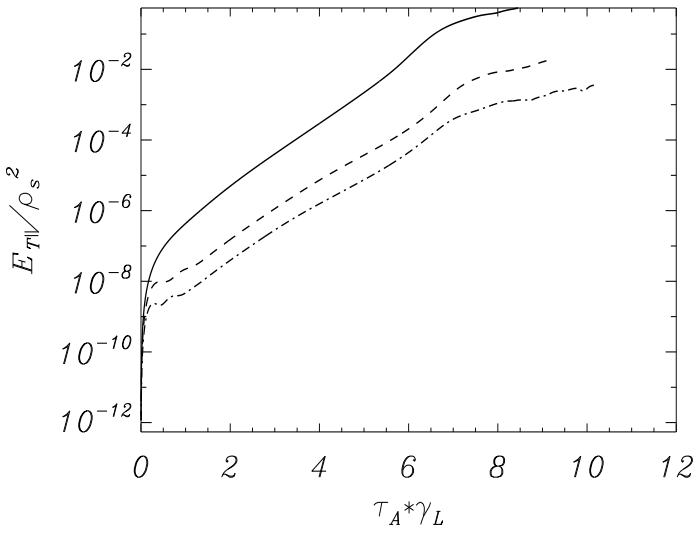

FIGURE 5. Evolution in time of the energy associated with the parallel temperature variations for three different values of ρ_s; $\rho = 0.01$ (solid line), $\rho_s = 0.4$ (dashed line) and $\rho_s = 0.8$ (dashed-dotted line). We observe that triggering heat flux, by increasing the value of ρ_s, implies a reduction of temperature fluctuations.

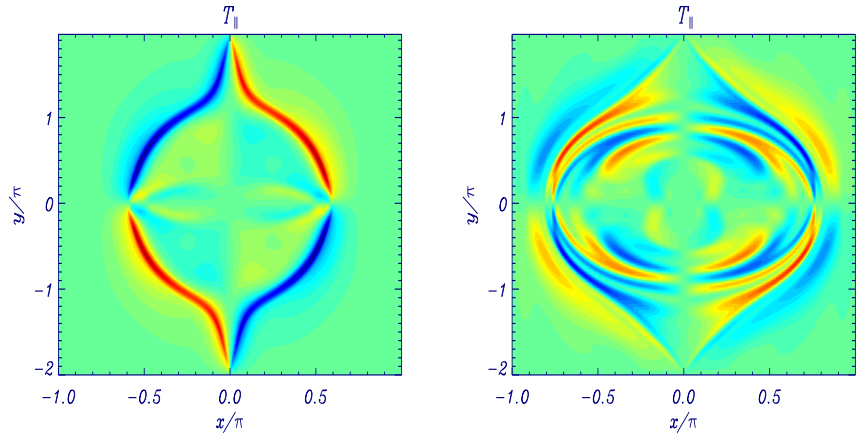

FIGURE 6. Contour plot of the parallel temperature fluctuations $T_\parallel$ for $\rho_s = 0.01$ (left panel) and $\rho_s = 0.8$ (right panel). For $\rho_s \ll d_e$, $T_\parallel$ distributes along the separatrices, similarly to n_e (compare with the left panel of Fig. 8). For larger ρ_s, temperature fluctuations reduce and distribute more uniformly inside the island.

to vorticity fluctuations. In the large ρ_s limit, as already noticed, the heat flux breaks the proportionality between n_e and $T_\parallel/2$. Whereas the former remains mainly concentrated along the separatrices, little energy is available for temperature fluctuations, which tend to be uniformly distributed inside the island.

6. Role of the Lagrangian invariants

In this section we investigate the role, on the reconnection process, of the Lagrangian invariants of the model, introduced in Sec. 3. The Lagrangian invariant dynamics underlying collisionless reconnection has already been exploited in two-, three- and four-field models for Hamiltonian reconnection such as those studied in Refs. (Cafaro *et al.* 1998; Grasso *et al.* 2001, 2010, 2009; Comisso *et al.* 2012). In all of these models some field variables (typically densities, parallel canonical momenta or vorticity) could be expressed as linear combination of two Lagrangian invariants associated with Casimirs of the corresponding Poisson brackets. The dynamics of the Lagrangian invariants could then be used as a viewpoint alternative to that of the original field variables. The inclusion of parallel temperature and heat flux fluctuations in the six-field model extends this picture. Indeed, by inverting the relations (3.16)-(3.19) one obtains

$$n_e = -\frac{G_1 - G_2 - (\sqrt{2}+\sqrt{3})(G_3 - G_4)}{4\sqrt{3+\sqrt{6}}d_e\rho_s},, \tag{6.1}$$

$$F = \frac{G_1 + G_2 + G_3 + G_4}{4}, \tag{6.2}$$

$$T_\parallel = -\frac{(\sqrt{2}+\sqrt{3})(G_1 - G_2) + G_3 - G_4}{2\sqrt{2}\sqrt{3+\sqrt{6}}d_e\rho_s}, \tag{6.3}$$

$$q_\parallel = -\sqrt{3}\frac{G_1 + G_2 - G_3 - G_4}{4\sqrt{2}d_e^2}, \tag{6.4}$$

$$n_i = \frac{I_+ - I_-}{2d_i\rho_i}, \tag{6.5}$$

$$D = \frac{I_+ + I_-}{2d_i\rho_i}. \tag{6.6}$$

The ion fields n_i and D remain linear combinations of two contributions $I_\pm$, as in the four-field model (Waelbroeck & Tassi 2012). The four electron fields, on the other hand, are all linear combinations of the four Lagrangian invariants G_1, G_2, G_3 and G_4. In particular we remark that n_e and $T_\parallel$ can be seen as linear combinations of the two fields $G_1 - G_2$ and $G_3 - G_4$, weighted with different coefficients. On the other hand, F and $q_\parallel$ can be seen as linear combinations of the two fields $G_1 + G_2$ and $G_3 + G_4$. Such two fields contribute to F and $q_\parallel$ with the same weight (up to the sign).

We observe that the field variables possess also discrete symmetries. The symmetries for the even-order moments n_e, $T_\parallel$ and n_i are

$$n_e(-x,y,t) = -n_e(x,y,t), \qquad n_e(x,-y,t) = -n_e(x,y,t), \tag{6.7}$$

$$T_\parallel(-x,y,t) = -T_\parallel(x,y,t), \qquad T_\parallel(x,-y,t) = -T_\parallel(x,y,t), \tag{6.8}$$

$$n_i(-x,y,t) = -n_i(x,y,t), \qquad n_i(x,-y,t) = -n_i(x,y,t), \tag{6.9}$$

whereas the symmetries for the odd-order moments are

$$F(-x,y,t) = F(x,y,t), \qquad F(x,-y,t) = F(x,y,t), \tag{6.10}$$

$$q_\parallel(-x,y,t) = q_\parallel(x,y,t), \qquad q_\parallel(x,-y,t) = q_\parallel(x,y,t), \tag{6.11}$$

$$D(-x,y,t) = D(x,y,t), \qquad D(x,-y,t) = D(x,y,t). \tag{6.12}$$

Such symmetries, through the linear combinations (3.16)-(3.20), reflect in the following relations between the Lagrangian invariants:

$$G_1(-x,y,t) = G_2(x,y,t), \qquad G_1(x,-y,t) = G_2(x,y,t), \tag{6.13}$$

$$G_3(-x,y,t) = G_4(x,y,t), \qquad G_3(x,-y,t) = G_4(x,y,t), \tag{6.14}$$

$$I_+(-x,y,t) = I_-(x,y,t), \qquad I_+(x,-y,t) = I_-(x,y,t). \tag{6.15}$$

In Ref. (Comisso *et al.* 2012), simulations of the four-field model showed that the two Lagrangian invariants associated with the electron fluid tend to rotate in opposite directions, under the action of stream functions analogous to those of Eqs. (3.22). For the Lagrangian invariants associated with the ion fluid, the rotations were greatly reduced as a consequence of the mass ratio. In the six-field model we confirm, without showing it, the same behavior with regard to the ion variables n_i and D. We focus then on the electron field variables, whose dynamics can be equivalently described by that of the Lagrangian invariants G_1, G_2, G_3 and G_4, following Eqs. (6.1)-(6.4). In Fig. 7 contour plots of the Lagrangian invariants G_1 and G_3 are shown (the contours plot of G_2 and

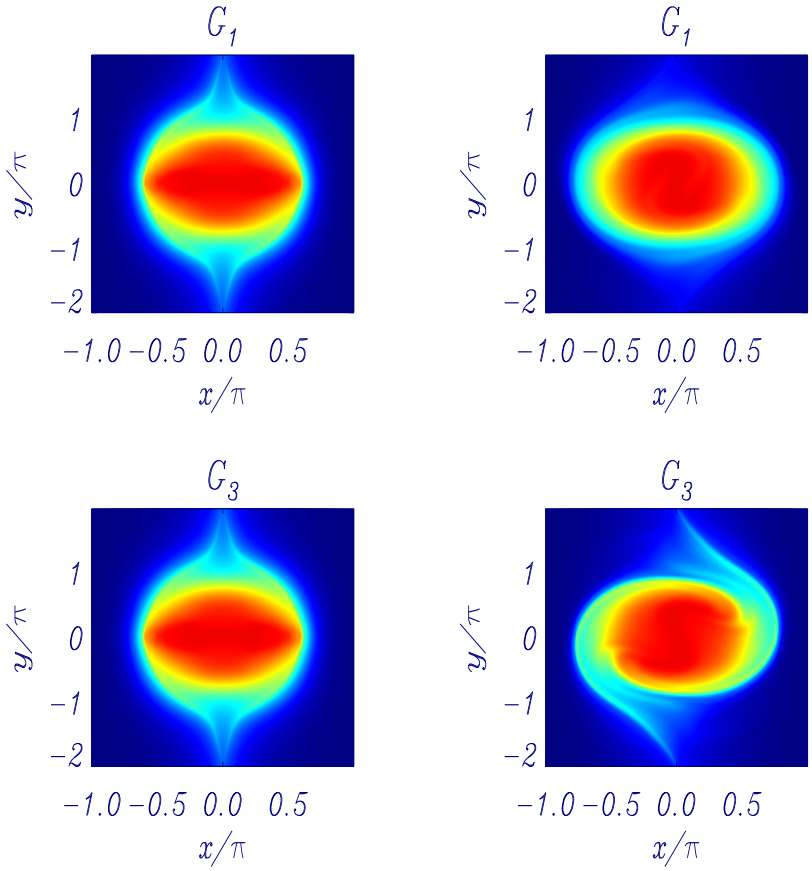

FIGURE 7. Contour plot of the invariants $G_{1,3}$ for $\rho_s = 0.01$ (left panel) and $\rho_s = 0.8$ (right panel). For $\rho_s = 0.8$ one can observe in the plot of G_3 the presence of two spiral arms, which are a signature of the rotation of the Lagrangian invariant. For $\rho_s = 0.01$ rotations in opposite directions of the two pairs of Lagrangian invariants tend to be suppressed.

G_4 can be obtained by reflection exploiting the symmetry properties discussed above). By looking in particular at the contour plot, for $\rho_s = 0.8$, of $G_{3,4}$, one observes two sorts of spiral arms which turn out to be essentially aligned with the island separatrices. These spiral arms are the result of a rotation of $G_{3,4}$ induced by the stream function $\phi_{3,4}$. Analogously, $G_{1,2}$ rotate in opposite directions under the action of the stream functions $\phi_{1,2}$. For the case $\rho_s = 0.01$ the rotations in opposite directions are essentially negligible because for $\rho_s \ll d_e$ one has $\phi_{1,2,3,4} \approx \phi$.

We can then reinterpret qualitative features of field structures in terms of the Lagrangian invariants. For the parallel temperature, for instance, the rotation of the invariants for $\rho_s = 0.8$ leads to the homogeneization of the fluctuations inside the island, as observed in Fig. 6. The absence of rotation for the case $\rho_s = 0.01$, on the contrary, leads to the persistence of structures clearly aligned with the island separatrix.

As above observed, the electron density is also given by a linear combination of $G_1 - G_2$ and $G_3 - G_4$, as the parallel temperature, but with different coefficients. Whereas for $T_\parallel$ the dominating contribution in the linear combination is $G_1 - G_2$, for the density it comes from $G_3 - G_4$ which is multiplied times the greater coefficient (and also subtracted).

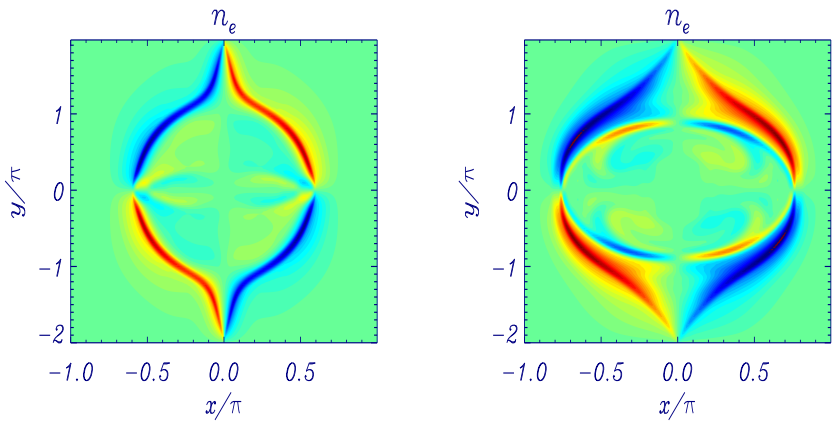

FIGURE 8. Contour plot of the electron density fluctuations n_e for $\rho_s = 0.01$ (left panel) and $\rho_s = 0.8$ (right panel). The distribution of the density fluctuations can be obtained as superposition of those of $G_1 - G_2$ and $G_3 - G_4$, according to Eq. (6.1).

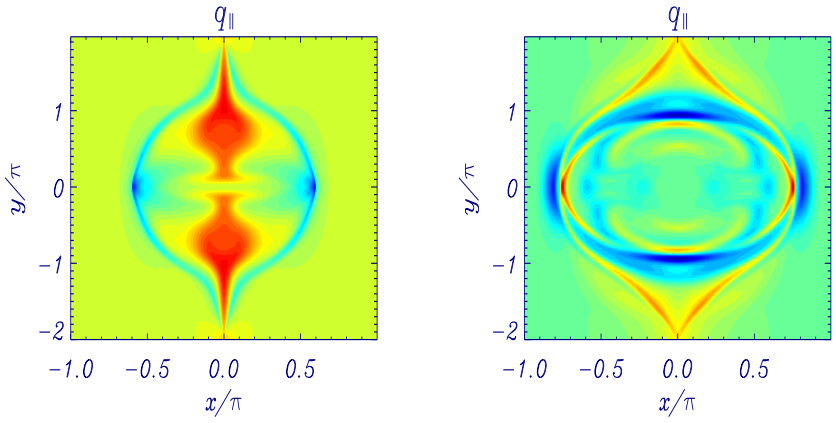

FIGURE 9. Contour plot of the heat flux fluctuations $q_\parallel$ for $\rho_s = 0.01$ (left panel) and $\rho_s = 0.8$ (right panel). Heat flux structures can be obtained as superposition of the structures of $G_1 + G_2$ and $G_3 + G_4$ according to Eq. (6.4). We note in particular the concentration along the separatrices, as a result of the opposite rotations of the Lagrangian invariants in the case $\rho_s = 0.8$.

This reflects in the electron density not having small scale structures inside the island for $\rho_s = 0.8$ (see Fig. 8), unlike $T_\parallel$. The absence of rotation for $\rho_s = 0.01$ amounts to yielding the same structures for n_e and $T_\parallel$, which corresponds, as observed in Sec. 5, to negligible heat flux.

The qualitative structures of the heat flux fluctuations can also be reinterpreted in terms of the Lagrangian invariants. We recall that in Sec. 5 we remarked that $q_\parallel$, when non-negligible, exhibits peaks around the separatrices. This can be observed also in Fig. 9 in the case $\rho_s = 0.8$. Such peaks reflect the superposition of the spiral arms of the invariants $G_{1,2,3,4}$ formed as a consequence of their rotation. When the rotation is essentially absent, as is the case for $\rho_s = 0.01$, such peaks are not present and the little amount of energy in the heat flux fluctuations is concentrated, to a large extent, also inside the island around the resonant surface $x = 0$.

7. Conclusions

We considered a six-field fluid model for collisionless reconnection accounting for electron parallel temperature and heat flux dynamics. The model extends previous Hamiltonian reconnection models (Cafaro *et al.* 1998; Waelbroeck *et al.* 2009; Waelbroeck & Tassi 2012) based on an isothermal closure. We showed that, like its isothermal predecessors, also the six-field model possesses a Hamiltonian structure with a noncanonical Poisson bracket. With regard to this point we mention that conservation of the total energy (the Hamiltonian functional) for the six-field model was already evident from Ref. (Scott 2010). Also, the property of energy conservation of the six-field model is compatible with the analysis of Ref. (Hammett *et al.* 1993). In this reference it is indeed pointed out that fluid models evolving a finite number $\mathcal{N}$ of moments of the Vlasov distribution function with respect to Hermite polynomials of the velocity coordinate, conserve energy if the hierarchy of fluid equations is closed setting the moment of order $\mathcal{N}+1$ equal to zero. The six-field model can actually be shown to admit a derivation from gyrokinetic equations by taking moments with respect to Hermite polynomials (Scott 2010) in the parallel velocity coordinate, and imposing the fourth-order moment to be zero. In this paper we have shown that the model, in addition to be energy-conserving, possesses the stronger property of being Hamiltonian. In particular, the noncanonical nature of the Poisson bracket implies, in addition to energy conservation, the existence of an infinite number of conserved functionals, corresponding to the Casimirs (3.14)-(3.15). Similarly to what occurred for the isothermal models (Cafaro *et al.* 1998; Waelbroeck *et al.* 2009; Waelbroeck & Tassi 2012), also in the six-field model then, in spite of the violation of the conservation of the topology of the magnetic field, alternative topological conservation laws constrain the dynamics. All contour lines of the Lagrangian invariants $G_{1,2,3,4}, I_{\pm}$ are indeed conserved, in spite of reconnection of magnetic field lines.

By means of numerical simulations we have observed that, when compared to the isothermal four-field model (Comisso *et al.* 2012), the six-field model yields, in the large Δ' regime, slightly greater linear growth rates, but essentially the same island saturation amplitudes, in agreement with hybrid fluid/kinetic models (Loureiro *et al.* 2013). In this respect, the effect of the heat flux on the reconnection process seems not to be considerable, at least for a plasma with no density or temperature equilibrium gradients, such as that considered in this paper.

Heat flux and parallel temperature offer new forms where energy can be converted to, when compared with the isothermal models. Indeed we observed that temperature and heat flux fluctations gain energy at the expense of electron thermal, electrostatic and parallel kinetic energies.

We also investigated the dynamics of the six-field model as function of the ρ_s parameter (or, equivalently, of the β_e parameter). For $\rho_s \ll d_e$ heat flux is negligible and consequently temperature fluctuations tend to go in phase with density fluctuations. In particular they both concentrate along the island separatrices. Increasing the value of ρ_s triggers heat flux fluctuations which, as expected, act to damp temperature fluctuations. The latter, in particular, tend to distribute more uniformly inside the island. This occurs as a consequence of heat flux distributing along the separatrices. Density fluctuations too, still exhibit a considerable concentration along the separatrices.

The field structures can also be qualitatively reinterpreted in terms of the Lagrangian invariants as done in Refs. (Cafaro *et al.* 1998; Grasso *et al.* 2001; Comisso *et al.* 2012). In particular, it emerged that the four electron variables n_e, F, $T_\parallel$ and $q_\parallel$ organize in pairs according to their discrete symmetry properties. n_e and $T_\parallel$, which are odd functions, appear as linear combinations of $G_1 - G_2$ and $G_3 - G_4$. On the other hand, the even

fields F and $q_\parallel$ are proportional to the sum and the difference, respectively, of $G_1 + G_2$ and G_3+G_4. Rotation of the Lagrangian invariants $G_{1,2,3,4}$ is observed as was the case for the Lagrangian invariants of isothermal models. In particular, for large ρ_s, the rotation induces the formation of structures similar to spiral arms, along the separatrices, in G_3 and G_4. For $\rho_s \ll d_e$, on the other hand, little stretching of the invariants is observed, due to the negligible influence of the magnetic potential in the advecting stream functions $\phi_{1,2,3,4}$. Above mentioned features of the field structures, such as the concentration of density and heat flux along the separatrices, can then be seen as the superposition of the Lagrangian invariants undergoing more or less intense stretching depending on the value of ρ_s. Rotation of the Lagrangian invariants had already been observed for the Hamiltonian isothermal models (Cafaro *et al.* 1998; Grasso *et al.* 2001; Comisso *et al.* 2012) and drift-kinetic systems (Liseikina *et al.* 2004; Pegoraro *et al.* 2005a,b). Our analysis shows that this feature persists when including parallel temperature and heat flux effects while preserving the Hamiltonian structure of the model.

ET acknowledges financial support from the Agence Nationale de la Recherche (ANR GYPSI n. 2010 BLAN 941 03) and from the CNRS through the PEPS project GEOPLASMA 2.

REFERENCES

Biskamp D. 2000 Magnetic Reconnection in Plasmas, *Cambridge University Press.*

Cafaro E. *et al.*1998 *Phys. Rev. Lett.* **80**, 4430.

Comisso L., Grasso D, Tassi E. & Waelbroeck F. L. 2012 *Phys. Plasmas* **19**, 042103.

Coppi B. 1964 *Phys. Lett.* **11**, 226.

de Blank H. J. 2001 *Phys. Plasmas* **8**, 3927.

Del Sarto D., Califano F. & Pegoraro F. 2006 *Mod. Phys. Lett. B* **20**, 931.

Fitzpatrick R. & Porcelli F. 2004 *Phys. Plasmas* **11**, 4713 and Erratum 2007 *Phys. Plasmas* **14**, 049902.

Furth H. P., Killen J. & Rosenbluth M. N. 1963 *Phys. Fluids* **6**, 459.

Grasso D., Califano F., Pegoraro F. & Porcelli F. 2000 *Plasma Phys. Rep.* **26**, 548.

Grasso D., Califano F., Pegoraro F. & Porcelli F. 2001 *Phys. Rev. Lett.* **86**, 5051.

Grasso D., Borgogno D., Pegoraro F. & Tassi E. 2009 *Nonlin. Processes Geophys.* **16**, 241.

Grasso D., Tassi E. & Waelbroeck F. L. 2010 *Phys. Plasmas* **17**, 082312.

Hammett G. W. *et al.* 1993 *Plasma Phys. Control. Fusion* **35**, 973.

Hazeltine R. D., Hsu C. T., & Morrison P. J. 1987 *Phys. Fluids* **30**, 3204.

Hesse M., Kuznetsova M. & Birn J. 2004 *Phys. Plasmas* **11**, 5387.

Holm D. D., Marsden J. E., Ratiu T. S. & Weinstein A. 1985 *Phys. Rep.* **123**, 1.

Kuvshinov B. N., Pegoraro F. & Schep T.J 1994 *Phys. Lett. A* **191**, 296.

Liseikina T. V., Pegoraro F. & Echkina E. Yu. 2004 *Phys. Plasmas* **11**, 3535.

Loureiro N. F. , Schekochihin A. A. & Zocco A. 2013 *Phys. Rev. Lett.* **111**, 025002.

Morrison P.J 1998 *Rev. Mod. Phys.* **70**, 467.

Pegoraro F., Liseikina T. & Echkina E. Yu. 2005a *Transport Theory and Statistical Physics* **34**, 243.

Pegoraro F., Liseikina T. & Echkina E. Yu. 2005b *Phys. Scripta* **T116**, 88.

Porcelli F. 1991 *Phys. Rev. Lett.* **66**, 425.

Priest E. R. & Forbes T. G. 2000 Magnetic Reconnection: MHD Theory and Applications, *Cambridge University Press.*

Schep T. J., Pegoraro F. & Kuvshinov B. N. 1994 *Phys. Plasmas* **1**, 2843.

Scott B. 2010 *Phys. Plasmas* **17**, 102306.

Snyder P.B. & Hammett G. W. 2001 *Phys. Plasmas* **8**, 3199.

Tassi E., Morrison P. J., Waelbroeck F.L. & Grasso D. 2008 *Plasma Phys. and Control. Fusion* **50**, 085014.
Tassi E., Morrison P. J., Grasso D. & Pegoraro F. 2010 *Nucl. Fusion* **50**, 034007.
Tassi E. 2014a *J. Phys. Conf. Series* **561** 012018.
Tassi E. 2014b *J. Phys. A: Math. Theor.* **47** 195501.
Thiffeault J.-L. & Morrison P. J. 2000 *Physica D* **136**, 205.
Waelbroeck F. L., Morrison P. J. & Horton W. 2004 *Plasma Phys. and Control. Fusion* **46**, 1331.
Waelbroeck F. L., Hazeltine R. D. & Morrison P. J. 2009 *Phys. Plasmas* **16**, 032109.
Waelbroeck F. L. & Tassi E. 2012 *Commun. Nonlinear Sci. Numer. Simulat.* **17**, 2171.
Yamada M, Kulsrud R. & Ji H. 2010 *Rev. Mod. Phys.* **82**, 603.
Zocco A. & Schekochihin A. A. 2011 *Phys. Plasmas* **18**, 102309.